Građevinski materijali i konstrukcije
Building Materials and Structures
journal homepage: www.dimk.rs

https://doi.org/10.5937/GRMK2500001D

Original scientific paper

Assessment of the development of strains/cracks in carbon-short-fiber-reinforced concrete (CSFRC) under static tensile loading using strain gauges and light-beam micrometer

Ante Džolan[*1)], Oliver Fischer[2)], Marino Jurišić[3)]

[1)] *Department of Structural Engineering, Faculty of Civil Engineering, University of Rijeka, 51000 Rijeka, Croatia*
[2)] *Chair of Concrete and Masonry Structures, Technical University of Munich, 80333 Munich, Germany*
[3)] *Department of Mechanics, Materials and Structures, Faculty of Civil Engineering, Architecture, and Geodesy, University of Mostar, 88000 Mostar, Bosnia and Herzegovina*

Article history
Received: 10 January 2025
Received in revised form: 04 February 2025
Accepted: 12 February 2025
Available online: 10 March 2025

Keywords
CSFRC,
light-beam micrometer (LBM),
ductile behavior,
strain, crack

ABSTRACT

Concrete is the most widely used material in the world today, but its extensive use also poses environmental risks due to high CO_2 emissions. To mitigate these emissions, reducing concrete consumption in construction is crucial. Enhancing its mechanical properties, particularly low tensile strength, can accomplish this. Enhancing tensile strength allows for the construction of smaller cross-sections of concrete elements, resulting in more efficient material utilization. One effective method for strengthening concrete is through fiber reinforcement. In this study, short carbon fibers are used to reinforce the concrete, creating a material known as short-carbon-fiber-reinforced concrete (CSFRC). The objective of this research is to advance the understanding of CSFRC's behavior under tensile stress. To do this, strain gauges and a light-beam micrometer (LBM) are used to track crack and strain growth, which gives information about how well the CSFRC is working overall.

1 Introduction

Buildings, bridges, and other infrastructure are essential for modern society to function effectively. Different types of infrastructure require various construction materials, with concrete being one of the most important. According to some sources, concrete is the most widely used man-made material and the second most used material overall, after water [1]. As a result, global concrete production has reached approximately 30 billion tons annually [2]. However, this extensive use of concrete has significant environmental consequences, as it accounts for 4 to 8% of total CO_2 emission [3]. To mitigate concrete's environmental impact, it is crucial to reduce the quantity of concrete used in construction. This can be achieved by minimizing concrete cross-sections, which requires addressing its main weakness—low tensile strength. The higher the tensile strength of concrete, the less material is needed for construction.

The tensile strength of concrete can be enhanced by incorporating various fibers (such as natural, steel, PVA, cellulose, glass fibers, etc.) into the fresh concrete mixture during the mixing process [4-17]. In this study, the addition of carbon fibers during the mixing phase improves the mechanical properties of concrete.Carbon fibers possess several advantageous characteristics, including the ability to withstand high stresses under both quasi-static and dynamic loading conditions, a high elastic modulus, creep resistance, low specific weight, high tensile strength, non-corrosiveness, a low thermal expansion coefficient, chemical stability, high thermal conductivity, and low electrical resistivity [18-21]. Due to their low electrical resistivity, concrete reinforced with carbon fibers also exhibits low electrical resistivity (i.e., high electrical conductivity). This makes carbon-fiber-reinforced concrete self-sensing, which lets cracks be found and concrete degradation be evaluated without damaging the concrete [22–31]. For this reason, some researchers refer to carbon-fiber-reinforced concrete as "smart concrete." In addition to these sensing capabilities, the inclusion of carbon fibers enhances the mechanical properties of concrete, as detailed below.

Concrete generally has significantly higher compressive strength than tensile strength, but the addition of carbon fibers further enhances its compressive strength. In [32], the design of M25 grade concrete, with a compressive strength of 28.13 MPa, followed IS 10262-2009 was used as the reference concrete. Specimens reinforced with 0.75 vol%, 1.00 vol%, and 1.25 vol% of carbon fibers showed compressive strength increases of 46.80%, 60.00%, and 32.40%, respectively, compared to the reference concrete. The optimal result was observed with 1.00 vol% of carbon fibers. In [33], the reference concrete had a compressive strength of 43.80 MPa and was reinforced with carbon fibers ranging from 0 to 2.40 vol%. The greatest increase in

* Corresponding author:
E-mail address: ante.dzolan@uniri.hr

compressive strength was seen with 0.2 vol% of carbon fibers, achieving 90.10 MPa—an increase of 105.70%. But as the amount of carbon fibers went above 0.2 vol%, the compressive strength steadily went down. The lowest value (17.40 MPa) was found in the mixture with 2.40 vol% carbon fibers. Similarly, the results in [34] indicate that compressive strength increases only up to a certain carbon fiber content, beyond which it begins to decline. For instance, plain concrete with a compressive strength of 40.88 MPa increased to 46.40 MPa (13.50% increase) with 1.00 vol% carbon fibers. At 1.50 vol%, the strength was 41.66 MPa (1.91% increase), while 2.00 vol% resulted in 39.48 MPa (3.55% decrease).

It looks like these results show that there is not a single way to tell if carbon-fiber-reinforced concrete will get stronger because it depends on both the concrete mix and the type of carbon fibers that are used [21]. A higher content of carbon fibers does not automatically result in higher compressive strength, and there is concern about over-reinforcing concrete with carbon fibers. To avoid this, the optimal fiber content for each concrete mixture must be determined.

The tensile strength of concrete can be measured directly or indirectly (through splitting tensile strength tests). In reference [35], the carbon fiber content in the concrete mixture is expressed as the fiber-cement ratio (f-c ratio). Splitting tensile strength was measured for f-c ratios of 0%, 4%, 8%, and 12%. The results show a continuous increase in splitting tensile strength as the f-c ratio rises from 0% to 8%. The peak value, 4.60 MPa, is reached at an f-c ratio of 8%, representing a 62% increase compared to the f-c ratio of 0% (2.84 MPa). However, further increasing the f-c ratio reduces the beneficial effect of carbon fiber reinforcement, with the splitting tensile strength at a 12% f-c ratio dropping to around 4.25 MPa—a 7.60% decrease compared to the strength at 8%.

Similarly, the results in [34] show the splitting tensile strength for various fiber contents: 0 vol%, 0.50 vol%, 1.00 vol%, 1.50 vol%, and 2.00 vol%. A near-linear increase in splitting tensile strength is observed as carbon fibers are added, with the highest value of 3.42 MPa at 2.00 vol% of fibers, which represents a 132.60% increase over plain concrete. In [32], plain concrete has a splitting tensile strength of 3.20 MPa, which increases steadily as the carbon fiber content rises to 1.00 vol%. At this level, the splitting tensile strength reaches 5.00 MPa, an increase of 56.25%. But at 1.25 vol%, the strength drops to 3.50 MPa, which is only 9.40% more than plain concrete. This shows that the tensile strength decreases as the carbon fiber content rises above 1.00 vol%.

As with compressive strength, these findings suggest that there is an optimal carbon fiber content, beyond which the benefits diminish or even become negative. Also, the results in [36] show that concrete reinforced with carbon fibers has higher splitting tensile strengths of 16.30% compared to concrete reinforced with glass fibers and 12.80% compared to steel fibers.

In [21], the tensile strength of plain concrete, concrete reinforced with steel fibers (SF), Zoltek carbon fibers (zCF), Hexcel carbon fibers (hCF), and recycled carbon fibers (rCF) were measured directly. It turns out that concrete reinforced with rCF has a tensile strength of 6.89 MPa, which is about 27.80% higher than plain concrete (5.21 MPa), 4.60% higher than concrete reinforced with SF (6.58 MPa), 26.30% higher than concrete reinforced with hCF (5.29 MPa), and 26.40% lower than concrete reinforced with zCF (8.99 MPa). In [37, 38], the directly measured tensile strength of concrete reinforced with 1.00 vol% zCF is reported to be around 15.00 MPa. These studies used a high-performance concrete (HPC) mixture, which was then reinforced with carbon fibers. According to [39], the tensile strength of HPC alone is approximately 7.90 MPa, meaning the addition of zCF increases the tensile strength by 90.00%.

The findings in [21, 37, 38] reveal varying degrees of improvement in tensile strength depending on the type of concrete mixture and carbon fibers used. These improvements are significantly influenced by the alignment angle between the carbon fibers and the direction of applied loads (stresses) [20, 37, 40, 41]—the smaller the alignment angle, the greater the improvement in mechanical properties, including tensile strength.

References [32-35, 42] demonstrate the improvement of flexural strength through the reinforcement of concrete with carbon fibers. However, careful attention must be given to avoid over-reinforcing the concrete According to studies [32, 33, 35], the flexural strength goes up up to a certain point where the optimal amount of carbon fibers is reached. After that, the benefits start to fade, and too many fibers can even make the flexural strength lower than in plain concrete. According to [37], the flexural strength of carbon-fiber-reinforced concrete increases by approximately 2.70-fold and 4.65-fold for concrete containing 1.00 vol% and 3.00 vol% of carbon fibers, respectively, when the fiber alignment angle relative to the applied stress is 0°. However, when the alignment angle increases to 30°, the improvement is reduced to around 1.13-fold for 1.00 vol% and 1.57-fold for 3.00 vol%.

These results show that carbon fiber reinforcement has less of a positive effect as the angle between the fibers and the direction of stress increases. At a 30° alignment angle, the impact is minimal, while at angles up to 20°, the positive effects are still noticeable. Beyond 40°, no improvement in flexural strength is observed [37].

In addition to enhancing mechanical properties, reinforcing concrete with carbon fibers alters the behavior of carbon-fiber-reinforced concrete under tension. Specifically, carbon fibers bridge cracks in the concrete [21], contributing to the pseudo-ductile behavior of carbon-fiber-reinforced concrete under tension [37, 38, 43]. This study contributes to the further understanding of the pseudo-ductile behavior of carbon-fiber-reinforced concrete under tensile loading. To this end, dog-bone-shaped specimens reinforced with short carbon fibers (3 mm in length) were prepared for direct static tensile tests. Due to the short length of the fibers, this material is referred to as carbon-short-fiber-reinforced concrete (CSFRC). The static tests were performed on specimens of different ages at the time of loading (28 and 70 days). For each age group, three specimens were tested, and their strain during the tests was measured using two techniques—strain gauges and a light beam micrometer (LBM). When measuring with strain gauges, the strain is measured in one point (micro-region), so that the results of different strain gauges can disagree to each other and it cannot be expected that the results of a single strain gauge correctly describe the behaviour of the entire testing area. Therefore, four different strain gauges were attached to the specimens in the testing area, and the behaviour of the testing area is described by the average value of these four strain gauges. However, the question arises as to whether this method of describing the behaviour of the testing area based on the average results from different points is reliable. To test this, the LBM micrometre was also used to measure the strain in the testing area. In contrast to strain gauges, the LBM measures the strains in a larger area (in this work in the entire testing area) and not in one point. Therefore, its results

are more relevant for describing the behaviour of the testing area than the results obtained with strain gauges. The main objective of this work is to investigate the reliability of the description of the behaviour of the test area based on the average results of several strain gauges. For this purpose, the average results of strain gauges are compared with the results measured with LBM.

2 Materials and methods

2.1 Raw materials and mixing procedure

The raw materials for the preparation of the CSFRC specimens are listed in Table 1:

Table 1. List of raw materials

Component	Type of Component	wt%
Cement	Holcim Sulfo 52.5 R	34.70
Silica fume	Sika Silicol P	21.70
Quartz powder	SF 500	21.70
Quartz sand	H33	7.70
Water	--	11.70
Superplasticizer	BASF ACE 460	2.50
Carbon fibers	Zoltek (Toray) PX35, 3 mm	1.00 (vol%)

Carbon fibers were uniformly cut to a length of 3 mm, with the following properties: diameter of 7 µm, elastic modulus of 242 GPa, tensile strength of 4137 MPa, and ultimate tensile strain of 1.5%. To enhance the dispersion of the fibers in the concrete mixture and improve adhesion between the fibers and the concrete, the fibers were oxidatively heated for 2 hours in an open furnace at 425°C before being incorporated into the cement paste [19]. The addition of carbon fibers decreases the workability of the concrete [34, 42]. However, workability can be improved by adding a superplasticizer to the cement matrix prior to incorporating the carbon fibers [33, 44]. The superplasticizer also aids in achieving better dispersion of the carbon fibers within the concrete. Furthermore, the addition of silica fume to the concrete mixture enhances the interfacial adhesion and dispersion of the fibers [19, 45]. Care should be taken when adding silica fume, as it can negatively affect the concrete, such as increasing shrinkage [45-49]. To achieve high early strength in the concrete paste, CEM 52.5 R cement was selected as the binder. Other components of the concrete mixture included quartz powder, quartz sand, and water.The maximum grain size of the sand is 0.6 mm, making it suitable for use in 3D concrete printing.

The mixing process consists of several phases. In the first phase, all dry components—cement, quartz powder, quartz sand, and silica—were placed into the mixer and thoroughly mixed. Once the dry components were well combined, water and superplasticizer were gradually added. The mixing continued until the air content in the mixture was minimized. Afterward, carbon fibers were incorporated into the mixture, and two mixing cycles lasting approximately 30 to 45 seconds were conducted to ensure uniform dispersion.

2.2 Printing process and curing procedure

To achieve optimal alignment between the carbon fibers and the applied stresses, a 3D printing technique was employed for the production of the specimens [50]. After completing the mixing procedure, the concrete mixture was transported in plastic bags to a 3D printer developed at the Technical University of Munich (TUM) for specimen fabrication [51]. Good fiber alignment was accomplished by extruding the concrete mixture through a nozzle with a diameter of 4 mm (Figure 1a). As a result, the deviation in the angle between the carbon fibers and the tensile stresses remained primarily within the range of ±10° [37]. A more detailed description of the printing process can be found in [52, 53].

The tested specimens were shaped like dog bones, measuring approximately 445 mm in height, 100 mm in width at both the upper and lower ends, and 50 mm in width in the testing area, which was also 50 mm in height. The specimens had a consistent depth of 50 mm (Figure 1b).

After the specimens were produced, they were placed in formwork and kept in an environment with 100% relative humidity (RH) for 1 day. Subsequently, for the following 6 days, the specimens were cured underwater. Following this 7-day curing period, the specimens were stored in a controlled environment with an RH of 65±5% and a temperature of 20±2°C until the day of testing.

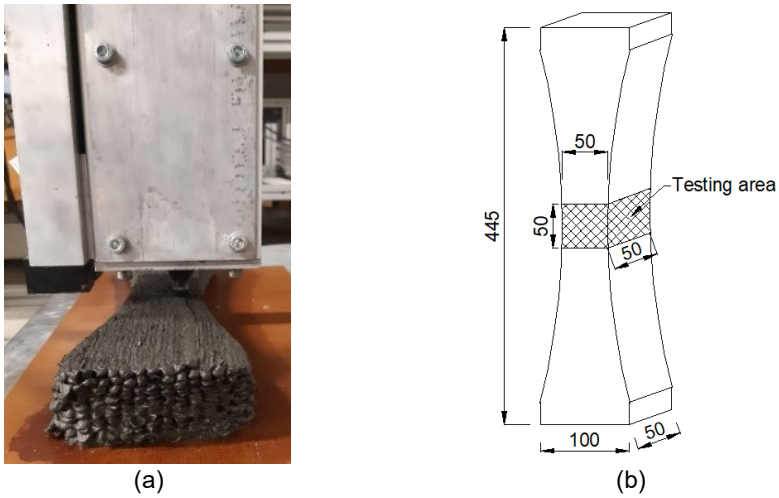

(a) (b)

Figure 1. Printing process (a); Shape and dimensions (measurement units are in mm) of the tested specimens (a) [38]

2.3 Testing procedure

One day before testing, strain gauges were attached to the specimens. Immediately afterward, the specimens were positioned in the testing device (Figure 2a). They were secured to the device using a two-component adhesive that required 24 hours to cure . Each specimen had four strain gauges put on it in the direction of the tensile load. Two gauges were placed on the top and bottom edges of the testing area (Figure 2b).

After the two-part glue had dried, two light beam micrometer (LBM) devices were attached to the test device and the samples (Figure 2) so the tests could begin.The specimens were subjected to uniaxial tensile loading in a displacement-controlled manner, with a loading rate of 0.003 mm/s. The load was gradually increased until the specimens fractured.

Three specimens were tested at 28 days of age, while another three specimens were tested at 70 days.

3 Results and discussion

3.1 Specimens tested at the age of 28 days

As mentioned earlier, four strain gauges were installed on each specimen to measure the development of strains. For the specimens loaded at 28 days, three specimens—designated as S37, S44, and S57—were tested. The results from all four strain gauges on specimen S57 are presented in Figure 3, from which an average line was derived.

Based on the average line, it is evident that the average first crack strength of specimen S57 (position A) is 9.11 MPa, corresponding to a strain of 0.24‰. The average ultimate tensile strength (position B) is 15.11 MPa, and the average ultimate tensile strain (position C) is 1.56‰ [38] (Figure 3). The average first crack strength, average tensile strength, and average ultimate tensile strain for specimens S37 and S44 were determined in the same manner and are presented in Table 2.

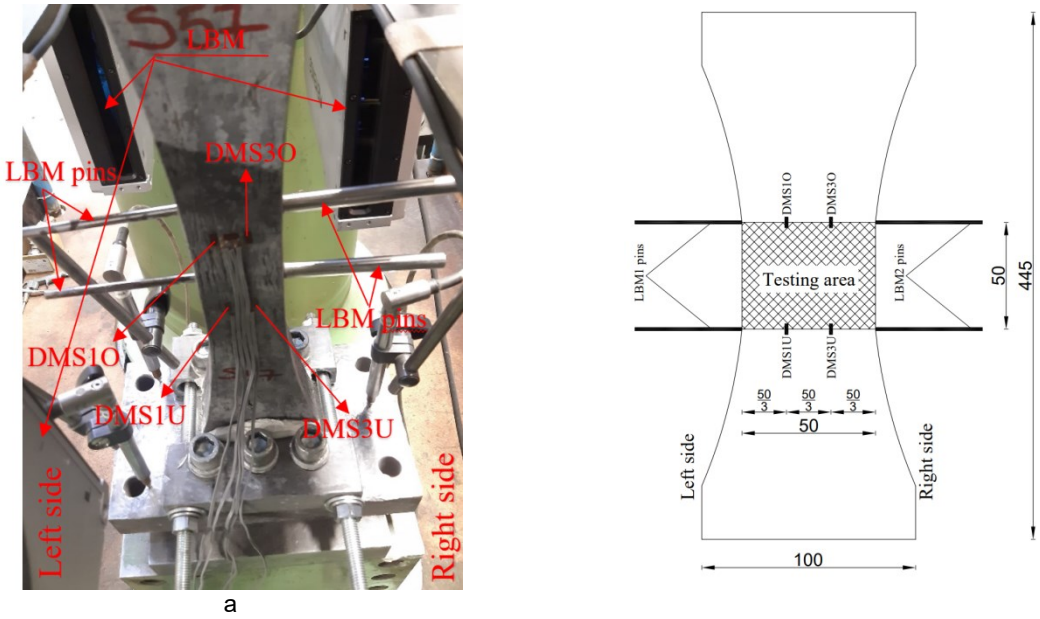

Figure 2. View of the specimen installed to the test device (a); Schematic representation of the measuring equipment's position (measurement units are in mm)(b)

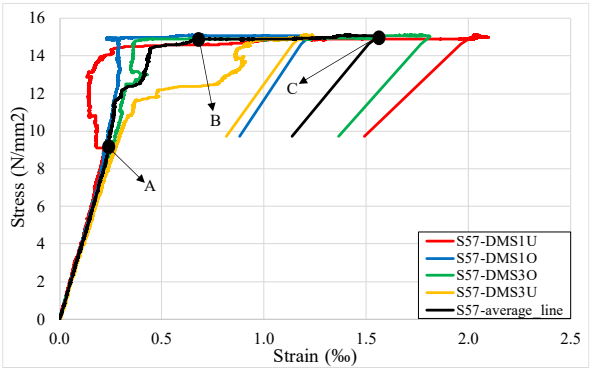

Figure 3. Results measured by strain gauges in the specimen S57

Table 2. Mechanical properties of the specimens S37 and S44 [38]

Specimen	First crack strength (MPa)	Tensile strength (MPa)	Ultimate tensile strain (‰)
S37	8.30	14.64	3.42
S44	9.20	15.01	2.28

Figure 4 presents a comparison of the average lines for all three specimens: S37, S44, and S57.

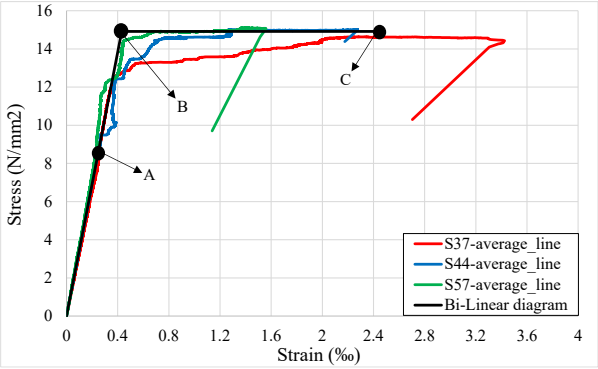

Figure 4. Stress-strain curves of the specimens loaded at the age of 28 days [38]

To see how carbon-short-fiber-reinforced concrete (CSFRC) acts when it is loaded at the age of 28 days [38], a bi-linear diagram can be made from the average lines.The bi-linear diagram indicates linear behavior until the stress reaches the tensile strength of 14.92 MPa [38] (position B in Figure 4), after which CSFRC yields until the ultimate tensile strength of 2.42‰ [38] (position C in Figure 4) is attained. However, Figure 4 reveals a slight discrepancy between the experimental results and the bi-linear diagram from position A (first crack strength of 8.87 MPa [38]) to position B. This discrepancy arises from micro-nonlinearity (micro-cracks) that occurs between positions A and B, which doesn't disrupt the global linearity of the specimens, i.e., the testing area. The strain measured by the strain gauge reflects the strain development at a specific point (a narrow local area), and the micro-nonlinearity at that point does not necessarily influence the global linearity of the specimen. This is evident in the results presented in Figure 3.

The blue (DMS1O) and green (DMS3O) lines in Figure 3 behave almost linearly until the tensile strength is reached. This means that there were no cracks at the locations of these two strain gauges or nearby. In contrast, the red line (DMS1U) demonstrates strain relaxation between positions A and B, suggesting that a micro-crack opened near the location of that strain gauge, leading to the observed strain relaxation. Unlike the red line, the yellow line (DMS3U) shows a sudden increase in strain at approximately 12.00 MPa. After the strain reaches around 0.80‰, the slope of the stress-strain curve closely resembles the slope before position A. This indicates that a micro-crack opened at the location of the strain gauge (reflected in the sudden increase of strain), which likely closed after some time as another micro-crack formed nearby.

The results presented in Figure 3 illustrate all possible types of strain development at the locations of the strain gauges. Similar trends were observed for specimens S37 and S44, which contributed to the average lines shown in Figure 4. These average lines are what the bi-linear diagram is built on, which lets us figure out how carbon-short-fiber-reinforced concrete (CSFRC) acts in a bigger picture.

A pertinent question arises: can these localized, somewhat mediocre results accurately predict the macro (i.e., global) behavior of CSFRC? To address this question, the results in Figure 4 are compared with those obtained using the light beam micrometer.

Figure 2 illustrates that the light beam micrometer (LBM) measures the distance—specifically, the change in distance—between the upper and lower edges of the testing area on both sides of the specimens during the tensile static test. From this distance change, the macro (i.e., global) strains (ΔL/L) of the testing area can be calculated. The LBM results for specimens S37 and S57 are presented in Figures 5a and 5b, respectively. However, specimen S44 experienced a lack of LBM data due to the LBM pins becoming unglued at the very beginning of the test.

Figures 5a and 5b present the LBM stress-strain curves alongside the bi-linear diagram from Figure 4. There is a strong link between the results when you look at the LBM curves (Figures 5a and 5b) and the average lines from the strain gauges (Figure 4).This indicates that the mediocre micro-results obtained from the strain gauges can reliably represent the global behavior of carbon-short-fiber-reinforced concrete (CSFRC), allowing the bi-linear diagram to serve as an effective tool for predicting CSFRC behavior. The coordinates of the bi-linear diagram are listed below:

Table 3. Coordinates of the bi-linear diagram.

Stress (MPa)	Strain (‰)
0.00	0.00
14.92	0.43
14.92	2.42

A comparison of the results in Figure 5 with those in Figure 3 clearly demonstrates that relying on data from a single strain gauge within the testing area is not sufficient for accurately predicting the behavior of carbon-short-fiber-reinforced concrete (CSFRC).

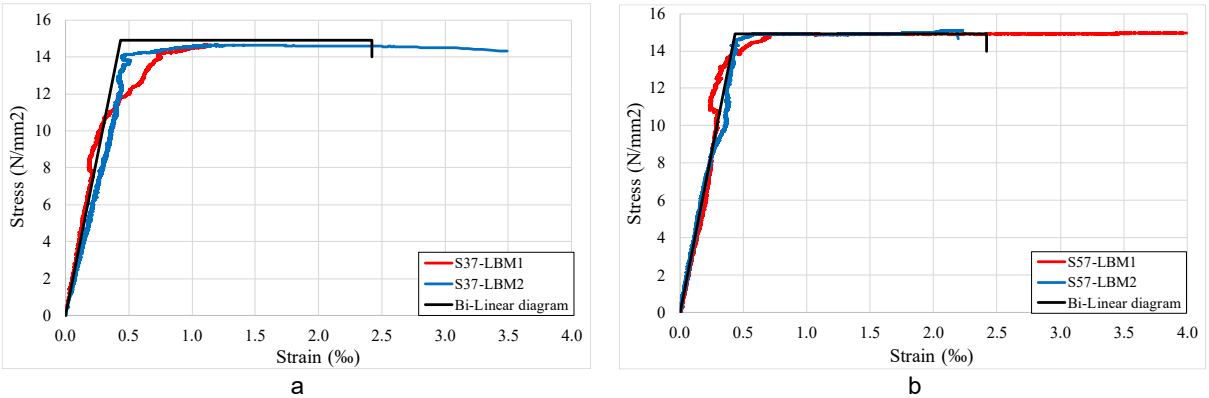

a b

Figure 5. LBM Stress-strain curves of the specimens S37 (a); and S57 (b)

3.2 Specimens tested at the age of 70 days

Specimens identified as S53, S56, and S59 were tested at 70 days of age. Figure 6 presents the results for specimen S56.

According to the results in Figure 6a, a linear relationship between stress and strain can be observed in all strain gauges until the stress reaches an average first crack strength of 11.35 MPa for the specimen [38]. After this point, strain relaxation occurs in all four strain gauges (Region A in Figure 6a). This strain relaxation indicates that the damage process—characterized by the opening of micro- and macro-cracks—occurs outside the testing area. This assertion is supported by Figure 6b, which shows that the main crack developed at the bottom edge of the testing area. The presence of these micro and macro cracks outside the testing area and along the specimen's edges fully relaxes the strain and crack state within the testing area. When the stress reaches the tensile strength of the specimen at 14.72 MPa, the CSFRC begins to yield (Figure 6a). The average ultimate strain for specimen S56 is recorded at 1.56‰ [38].

The failure of specimens S53 and S59 also occurred outside the testing area. In contrast to specimen S56, specimen S53's main crack formed well above the testing area (Figure 7a), while specimen S59's main crack formed well below the testing area (Figure 7b).

Since the main cracks in specimens S53 and S59 are located farther away from the testing area than in specimen S56, they do not relax the strain and crack state of specimens S53 and S59 as significantly as in specimen S56. This is illustrated in Figure 8, which presents the results for specimen S53.

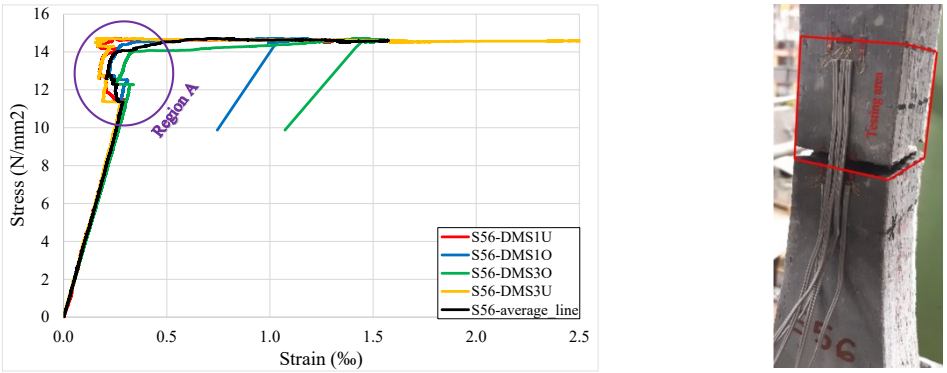

a b

Figure 6. Results measured by strain gauges in the specimen S56 (a); View of the specimen after failure (b)

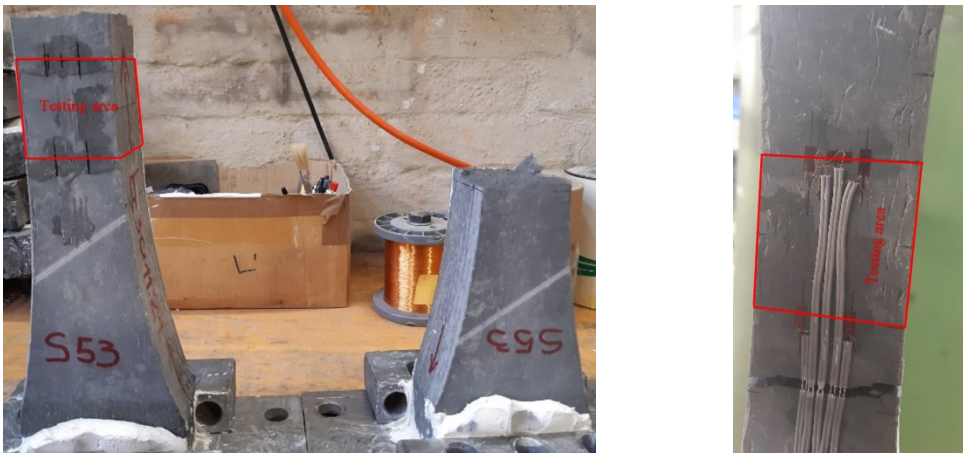

a b

Figure 7. View of the specimen S53 (a); and specimen S59 after failure (b)

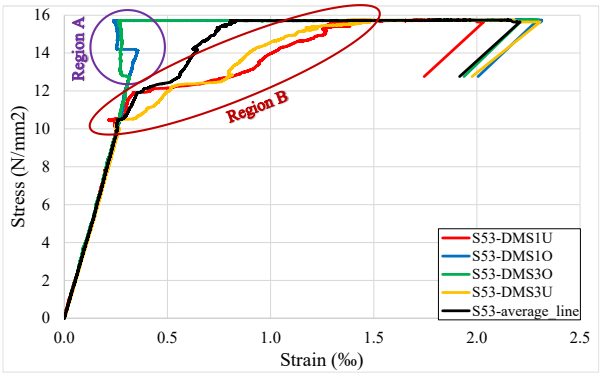

Figure 8. Results measured by strain gauges in the specimen S53

In region A (Figure 8), a soft relaxation of strains can be observed in the strain gauges DMS1O and DMS3O. These gauges are positioned closer to the main crack than DMS1U and DMS3U (Figure 7a). Therefore, the soft relaxation in these strains may be attributed to the proximity of the main crack to the strain gauges or the presence of micro- or macro-cracks nearby. In contrast, no relaxation effect is observed in strain gauges DMS1U and DMS3U.

Once the stress reaches the first crack strength (the average value for specimen S53 is 10.10 MPa [38]), the slope of the stress-strain curve in region B (Figure 8) is lower than before reaching the first crack strength. This means that global (macro) cracks are starting to appear at the locations of strain gauges DMS1U and DMS3U. These cracks keep getting bigger as the stress rises to the tensile strength (15.75 MPa [38]). Indeed, region B (Figure 8) indicates the hardening behavior of CSFRC when stress is between the first crack strength and the tensile strength. After the stress reaches the tensile strength, CSFRC begins to yield, and upon reaching the ultimate tensile strain (the average value for specimen S53 is 2.20‰), the specimen ultimately breaks.

The behavior of specimen S59 is similar to that of specimen S56, and its mechanical properties are provided in Table 4.

Table 4. Mechanical properties of the specimens S59 [38]

Specimen	First crack strength (MPa)	Tensile strength (MPa)	Ultimate tensile strain (‰)
S59	10.20	15.69	1.76

In Figure 9, alongside the average lines of the tested specimens, two prediction models—the bi-linear diagram and the stress-strain curve in four points—are also presented. The stress-strain curve in four points effectively simulates the experimental results of specimens S53 and S59. In contrast, the behavior of specimen S56 is more accurately represented by the bi-linear diagram. The coordinates of these two prediction models are provided in Table 5:

For each specimen, the average stress-strain curves were generated based on the results from four different strain gauges, as illustrated in Figure 9.

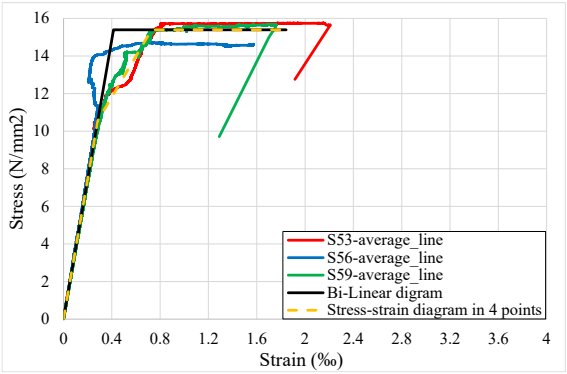

Figure 9. Stress-strain curves of the specimens loaded at the age of 70 days [38]

The results presented in Figure 9 are derived from averaging the data collected at various points, allowing for the prediction of the global (macro) behavior based on these local (micro) results. To validate the prediction models illustrated in Figure 9 and Table 3, a comparison is made between these results and those obtained through Light Beam Micrometer (LBM) measurements. The global (macro) results for the testing area of specimens S53 and S56, as obtained by LBM, are displayed in Figure 10. Unfortunately, for specimen S59, the LBM pins detached from the specimen at the beginning of the test, resulting in a lack of LBM data for this specimen.

Table 5. Coordinates of the bi-linear diagram

Bi-Linear diagram			***Stress-strain curve in 4 points***	
Stress (MPa)	Strain (‰)		Stress (MPa)	Strain (‰)
0.00	0.00		0.00	0.00
15.39	0.41		10.55	0.28
15.39	1.84		15.39	0.73
			15.39	1.84

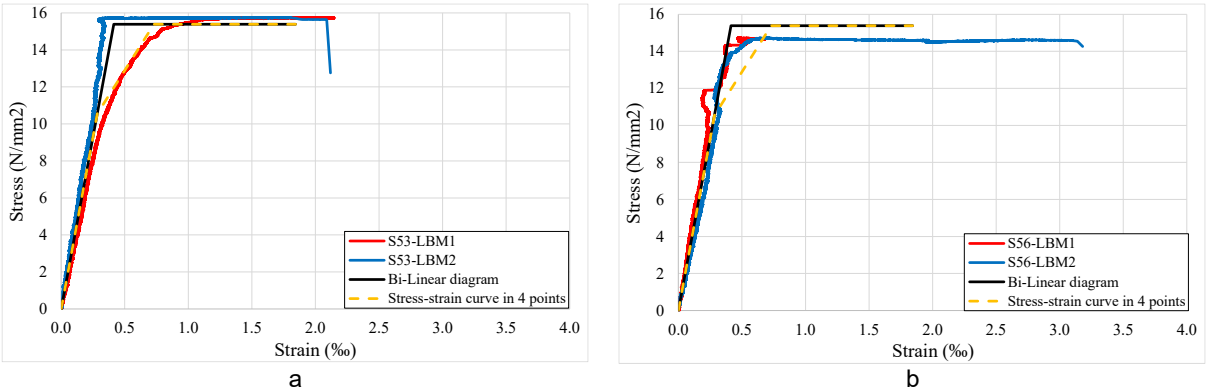

a b

Figure 10. LBM Stress-strain curves of the specimens S53 (a); and S56 (b)

The results in Figure 10a show that both the bi-linear diagram and the stress-strain curve in four points can accurately predict how Carbon-Short-Fiber-Reinforced Concrete (CSFRC) will behave on a larger scale. These are based on the local (micro) results from four different points in the testing area (shown in Figure 9). Additionally, Figure 10b confirms that the bi-linear diagram reliably characterizes the behavior of specimen S56.

The LBM results presented in Figure 10a reveal a distinct behavior between the left side of specimen S53 (LBM1) and the right side (LBM2). On the left side, the stress-strain curve remains nearly linear until the stress reaches the tensile strength, after which the CSFRC begins to yield. In contrast, the stress-strain curve on the right side is linear only until the stress hits the first crack strength. Following this, the CSFRC exhibits hardening while the stress is between the first crack strength and tensile strength. Once the tensile strength is achieved, the CSFRC starts to yield. This disparity in results between the left and right sides of the specimen suggests the location of the first global (macro) crack within the testing area and indicates the direction of its propagation. Specifically, the global crack in the testing area initiates on the right side of the specimens and propagates towards the left side as the load increases.

3.3 Comment on the CSFRC behavior

Based on the previously described results, CSFRC clearly demonstrates a highly ductile behavior under tension. However, notable differences in this behavior emerge concerning the age of the loaded specimens. Specifically, specimens loaded at the age of 28 days exhibit an almost linear behavior until the stress reaches the tensile strength. While the global behavior remains nearly linear, a local (micro) non-linearity can be observed in the testing area when the stress is between the first crack strength and the tensile strength. Once the stress surpasses the tensile strength, CSFRC begins to yield.

When the stress is between the first crack strength and the tensile strength, the specimens loaded at 70 days show a tendency for CSFRC to harden. This is not the case with the specimens loaded at 28 days. Accordingly, their behavior can be divided into three distinct phases. Initially, until the stress reaches the first crack strength, they exhibit a linear behavior. Once this happens, and the stress is between the first crack strength and the tensile strength, something similar to CSFRC hardening happens. Finally, after the stress surpasses the tensile strength, CSFRC begins to yield.

4 Conclusions

Based on the presented results, the following conclusions can be drawn:

- **HighTensile Strength**: Carbon-short-fiber-reinforced concrete (CSFRC) exhibits relatively high tensile strength, nearly twice that of high-performance concrete and approximately six times greater in comparison with normal-strength concrete.
- **Ductile Behavior**: CSFRC demonstrates highly ductile behavior, regardless of the age at the time of loading. This characteristic enhances its fatigue performance.
- **Prediction of 28-Day Behavior**: The behavior of CSFRC loaded at 28 days can be accurately predicted using a bi-linear diagram. This behavior can be divided into two distinct phases: a predominantly linear behavior until the tensile strength is reached, followed by yielding once the tensile strength is exceeded. While no global cracks are present before reaching the tensile strength, a network of micro-cracks (micro-nonlinearity) develops between the first crack strength and tensile strength, contributing positively to the fatigue performance of CSFRC.
- **70-Day Behavior**: In contrast, CSFRC loaded at 70 days exhibits a tendency toward CSFRC hardening when the stress is between the first crack strength and the tensile strength. This behavior can be reliably predicted using a stress-strain curve with four points, which is divided into three distinct phases: a linear behavior until reaching the first crack strength, CSFRC hardening indicating the opening of global cracks between the first crack strength and tensile strength, and yielding after reaching the tensile strength. The global cracks that form enhance the fatigue performance of CSFRC compared to the specimens loaded at 28 days.
- Prediction **of Global Behavior**: **Relying on a single strain gauge in the testing area to predict global (macro) behavior is not feasible.** Increasing the number of strain gauges improves the accuracy of predictions for global behavior. The global behavior predicted by averaging the results from four strain gauges aligns closely with the global results obtained from light-beam micrometers (LBM).
- **Utilizationof LBMs**: Employing two LBMs on opposite sides of the specimens facilitates the prediction of where the global crack will appear and the direction of its propagation.
- **Hardening of the testing area:** All three specimens tested at 28 days broke within the testing area, while those tested at 70 days broke outside the testing area. This indicates that the ageing of CSFRC has a positive effect on the hardening of the testing area and on the improvement of its energy dissipation capacity.
- **Limitations of the study and directions for future research:** This study investigared only the CSFRC with one amount of carbon fibers. It did not look at what happens when this material is reinforced with more carbon fibers.

Therefore, future research should shed light on how effective the reinforcement of concrete with carbon fibers is when the content of carbon fibers increases.

CRediT authorship contribution statement:

Project administration, O.F.; supervision, O.F.; writing-review and editing: O.F., A.D., M.J.; conceptualization, A.D.; data curation: A.D.; formal analysis investigation: A.D.; methodology: A.D.; visualization: A.D.; validation: A.D.; writing – original draft preparation: A.D., M.J. All authors have read and agreed to the published version of the manuscript.

Declaration of competing interest:

The funders had no role in the design of the study; in the collection, analyses or interpretation of data; in the writing of the manuscript or in the decision to publish the results.

Funding: This research is funded by the German Research Foundation (DFG) as part of the Priority Program SPP2020: “Cyclic deterioration of High-Performance Concrete in an experimental-virtual lab” (Grant Numbers FI1720/7-1, GR1664/13-1, PE1464/6-1, VO829/13-1)

Acknowledgments:

The researcher express their gratitude to everyone involved in the priority program SPP2020, as the working atmosphere between the groups is created by fruitful collaboration.

References

[1] Concrete: the most destructive material on Earth, https://www.theguardian.com/cities/2019/feb/25/concrete-the-most-destructive-material-on-earth (accessed on 2 October 2024).

[2] There Will Soon Be More Concrete Than Biomass on Earth, https://heatmap.news/economy/the-planet-s-jaw-dropping-astonishing-downright-shocking-amount-of-concrete (accessed on 2 October 2024).

[3] Environmental Go!: 9 Environmental impacts of Cement Production, https://hr.environmentgo.com/utjecaj-proizvodnje-cementa-na-okoli%C5%A1/#google_vignette (accessed on 2 October 2024).

[4] A.M.Brandt,Fibre reinforced cement-based (FRC) composites after over 40 years of development in building and civil engineering,*Compos. Struct.*86 (2008) 3–9. doi.org/10.1016/j.compstruct.2008.03.006

[5] X.Guo,G. Xiong, Resistance of fiber-reinforced fly ash-steel slag based geopolymer mortar to sulfate attack and drying-wetting cycles,*Constr. Build. Mater.*269 (2021) 121326. doi.org/10.1016/j.conbuildmat.2020.121326

[6] H.M.Hamad,J.Shi,M.S.Al Jawahery,A.Majdi,S.T.Yousif,G. Kaplan, Application of natural fibers in cement concrete: A critical review,*Mater. Today Commun.*35 (2023) 105833. doi.org/10.1016/j.mtcomm.2023.105833

[7] K.Hannawi,H.Bian,W.Prince-Agbodjan,B. Raghavan, Effect of different types of fibers on the microstructure and the mechanical behavior of Ultra-High Performance Fiber-Reinforced Concretes,*Compos. Part B Eng.*86 (2016) 214–220. doi.org/10.1016/j.compositesb.2015.09.059

[8] G.L.Insaurriaga,C.C.Gomes,F.V.Ribeiro,G.L.Calegaro ,T.A.Silveira,L.F.Cruz,J.A.Cruz,S.C.Amico,RA. Belucis, Effect of Hybridization of Carbon Fibers on Mechanical Properties of Cellulose Fiber-Cement Composites: A Response Surface Methodology Study,*C-J Carbon. Res.*10 (2024) 41. doi.org/10.3390/c10020041

[9] S.H.Kosmatka,W.C.Panarese,B. Kerkhoff, Design and Control of Concrete Mixtures. Portland Cement Association Skokie: Skokie, IL, USA, 2002; Volume 5420.

[10] I.L.Larsen,R.T. Thorstensen, The influence of steel fibres on compressive and tensile strength of ultra high performance concrete: a review,*Constr. Build. Mater.*256 (2020) 119459. doi.org/10.1016/J.CONBUILDMAT.2020.119459

[11] J.Liu,C. Lv, Durability of Cellulosic-Fiber-Reinforced Geopolymers: A Review,*Molecules.*27 (2022) 796. doi.org/10.3390/molecules27030796

[12] J.Liu,C. Lv, Properties of 3D-Printed Polymer Fiber-Reinforced Mortars: A Review,*Polym.*14 (2022) 1315. doi.org/10.3390/polym14071315

[13] J.Liu,C. Lv, Research progress on durability of cellulose fiber-reinforced cement-based composites,*Int. J.Polym. Sci.*2021 (2021) 1014531. doi.org/10.1155/2021/1014531

[14] L.Mohammed,M.N.M.Ansari,G.Pua,M.Jawaid,M.S. Islam, A review on natural fiber reinforced polymer composite and its applications,*Int. J.Polym. Sci.*2015 (2015) 1–15. doi.org/10.1155/2015/243947

[15] J.A.Sainz-Aja,M.Sanchez,L.Gonzalez,P.Tamayo,G.Garcia del Angel,A.Aghajanian,S.Diego,C. Thomas, Recycled Polyethylene Fibres for Structural Concrete,*Appl. Sci.*12 (2022) 2867. doi.org/10.3390/app12062867

[16] S.F.A.Shah,B.Chen,S.Y.Oderji,M.A.Haque,M.R. Ahmad, Comparative study on the effect of fiber type and content on the performance of one-part alkali-activated mortar,*Constr. Build. Mater.*243 (2020) 118221. doi.org/10.1016/j.conbuildmat.2020.118221

[17] P.Zhang,X.Han,Y.Zheng,J.Wan,D. Hui, Effect of PVA fiber on mechanical properties of fly ash-based geopolymer concrete,*Rev. Adv. Mater. Sci.*60 (2021) 418–437. doi.org/10.1515/rams-2021-0039

[18] S.C. Chen,X.L. Shi,X.M. Yu,Effect of voltage on mechanical properties of carbon fiber reinforced concrete,*J. Phys: Conf. Ser.*2680 (2024) 012022. doi:10.1088/1742-6596/2680/1/012022

[19] H.Gao,Y. Xia, Research on the dispersion of carbon fiber and recycled carbon fiber in cement-based materials: a review,*Front. Mater.*10 (2023) 1243392. doi.org/10.3389/fmats.2023.1243392

[20] T.V.Muthukumarana,M.A.V.H.M.Arachchi,H.M.C.C.So marathna,SN. Raman, A review on the variation of mechanical properties of carbon fiber-reinforced concrete,*Constr. Build. Mater.*366 (2022) 130173. doi.org/10.1016/j.conbuildmat.2022.130173

[21] A.Patchen,S.Young,D. Penumadu, An Investigation of Mechanical Properties of Recycled Carbon Fiber Reinforced Ultra-High-Performance Concrete,*Mater.*16 (2023) 314. doi.org/10.3390/ma16010314

[22] D.M. Bontea,D.D.L. Chung,G.C. Lee Damage in carbon fiber-reinforced concrete, monitored by electrical resistance measurement,*Cem.Concr. Res.*30 (2000) 651-659. doi.org/10.1016/S0008-8846(00)00204-0

[23] B.Chen,J. Liu, Damage in carbon fiber-reinforced concrete, monitored by both electrical resistance measurement and acoustic emission analysis,*Constr. Build. Mater.*22 (2008) 2196-2201. doi.org/10.1016/j.conbuildmat.2007.08.004

[24] P.W. Chen,D.D.L. Chung,Carbon fiber reinforced concrete for smart structures capable of non-destructive flaw detection,*Smart. Mater. Struct.*2 (1993) 22-30. doi.org/ 10.1088/0964-1726/2/1/004

[25] D.D.L. Chung, Cement reinforced with short carbon fibers: a multifunctional material,*Compos. B: Eng.*31 (2000) 511-526. doi.org/10.1016/S1359-8368(99)00071-2

[26] Y.Hao,C.Shi,Z.Bi,Z.Lai,A.She,W. Yao, Recent Advances in Properties and Applications of Carbon Fiber-Reinforced Smart Cement-Based Composites,*Mater.*16 (2023) 2552. doi.org/10.3390/ma16072552

[27] A.Loukidis,I.Stavrakas,D. Triantis, Electrical Methods for Sensing Damage in Cement Mortar Beams Combined with Acoustic Emissions,*Mater.*15 (2022) 4682. doi.org/10.3390/ma15134682

[28] Z.Q.Shi,D.D.L. Chung, Carbon fiber-reinforced concrete for traffic monitoring and weighing in motion,*Cem.Concr. Res.*29 (1999) 435-439. doi.org/10.1016/S0008-8846(98)00204-X

[29] M.Sun,Z.Li,Q.Mao,D. Shen, Thermoelectric percolation phenomena in carbon fiber-reinforced concrete,*Cem.Concr. Res.*28 (1998) 1707-1712. doi.org/10.1016/S0008-8846(98)00161-6

[30] M.Sun,Q.Liu,Z.Li,Y. Hu, A study of piezoelectric properties of carbon fiber reinforced concrete and plain cement paste during dynamic loading,*Cem.Concr.Res.*30 (2000) 1593-1595. doi.org/10.1016/S0008-8846(00)00338-0

[31] W.Wang,S.Wu,H. Dai, Fatigue behavior and life prediction of carbon fiber reinforced concrete under cyclic flexural loading,*Mater. Sci.Eng: A*434 (2006) 347-351. doi.org/10.1016/j.msea.2006.07.080

[32] H.A.Navya,N.N. Patil, Experimental studies on behaviour of carbon fiber reinforced concrete. *IJCIET*9 (2018) 1461.1469. https://iaeme.com/Home/issue/IJCIET?Volume=9&Issue=7

[33] J.Zhang,A.Heath,R.J.Ball,K. Paine, Effect of fibre loading on the microstructural, electrical, and mechanical properties of carbon fibre incorporated smart cement-based composites,*Front. Mater.*9 (2022)1055796. doi: 10.3389/fmats.2022.1055796

[34] S.Y.Ghanem,J. Bowling, Mechanical Properties of Carbon-Fiber-Rinforced Concrete,*Adv. Civ. Eng.Matls.*8 (2019) 224-234. doi.org/10.1520/ACEM20180089

[35] G.J.Liu,E.L.Bai,J.Y.Xu,N. Yang, Mechanical Properties of Carbon Fiber-Reinforced Polymer Concrete with Different Polymer-Cement Rations,*Mater.*12 (2019)3530. doi:10.3390/ma12213530

[36] O.S. Khan,S. Sohu,M.Z. Jamali,S.Ahmed,S. Nagapan,Improving mechanical properties of concrete by using fibrous materials,*Eng. Solid. Mech.*12 (2024)437-446. doi: 10.5267/j.esm.2024.4.001

[37] M. Rutzen,P. Lauff,R. Niedermeier,O. Fischer,M. Raith,C.U. Grosse, U. Weiss,M.A. Peter,D. Volkmer, Influence of fiber alignment on pseudoductility and microcracking in a cementitious carbon fiber composite material,*Mater. Struct.*54 (2021) 58. doi.org/10.1617/s11527-021-01649-2

[38] A.Džolan,P.Lauff,O.Fischer,G. Šunjić, Influence of Concrete Shrinkage on the Behavior of Carbon Short-Fiber-Reinforced Concrete (CSFRC) under Tension,*Appl. Sci.*13 (2023) 7081. doi.org/10.3390/app13127081

[39] Y.Kusumawardaningsih,E.Fehling,M.Ismail,A.A.M.Aboubakr, Tensile strength behaviour of UHPC and UHPFRC,*Procedia. Eng.*125 (2015) 1081-1086. doi.org/10.1016/j.proeng.2015.11.166

[40] M. Hambach,H. Möller,T. Neumann,D. Volkmer,Portland cement paste with aligned carbon fibers exhibiting exceptionally high flexural strength (>100 MPa),*Cem.Concr. Res.*89 (2016) 80–86. doi.org/10.1016/j.cemconres.2016.08.011

[41] P. Lauff,P. Pugacheva,M. Rutzen,U. Weiß,O. Fischer,D. Volkmer,M.A. Peter,C.U. Große,Evaluation of the Behavior of Carbon Short Fiber Reinforced Concrete (CSFRC) Based on a Multi-Sensory Experimental investigation and a Numerical Multiscale Approach,*Mater.*14 (2021) 7005. doi.org/10.3390/ma14227005

[42] V.Bellary,B.Khartode,M.Shewale,S.R.Arangi,N. Shinde, Experimental Investigation of Randomly Distributed Carbon Fibers in Concrete Beams,*E3S Web of Conf.*559 (2024) 04052. https://doi.org/10.1051/e3sconf/202455904052

[43] D.L.Nguyen,D.K.Thai,DJ. Kim, Direct tension-dependent flexural behavior of ultra-high-performance fiber-reinforced concretes,*J. Strain Anal. Eng. Des.*52 (2017) 121-134. doi.org/10.1177/0309324716689625

[44] M.Safiuddin,G.Abdel-Sayed,N. Hearn, Absorption and strength properties of short carbon fiber reinforced mortar composite,*Buildings*11 (2021) 300. doi.org/10.3390/buildings11070300

[45] S.Ivorra,P.Garces,G.Catala,L.G.Andion,E. Zornoza, Effect of silica fume particle size on mechanical properties of short carbon fiber reinforced concrete,*Mater. Des.*31 (2010) 1553–1558. doi.org/10.1016/j.matdes.2009.09.050

[46] P.W. Chen,D.D.L. Chung,Low-drying-shrinkage concrete containing carbon fibers,*Compos. B Eng.*27 (1996) 269–274. doi.org/10.1016/1359-8368(95)00020-8

[47] P.Lura,O.M.Jensen,K. van Breugel, Autogenous shrinkage in high-performance cement paste: An evaluation of basic mechanisms,*Cem.Concr. Res.*33 (2003) 223–232. doi.org/10.1016/S0008-8846(02)00890-6

[48] L.Wu,N.Farzadnia,C.Shi,Z.Zhang,H. Wang, Autogenous shrinkage of high performance concrete: A review,*Constr. Build. Mater.*149 (2017) 62–75. doi.org/10.1016/j.conbuildmat.2017.05.064

[49] L.Yang,C.Shi,Z. Wu, Mitigation techniques for autogenous shrinkage of ultra-high-performance concrete—A review,*Compos. B Eng.*178 (2019) 107456. doi.org/10.1016/j.compositesb.2019.107456

[50] V.N.Nerella,H.Ogura,V. Mechtcherine, Incorporating reinforcement into digital concrete construction. In Proceedings of the IASS Symposium 2018: Creativity in Structural Design, Boston, MA, USA, 16–20 July 2018.

[51] TUMuenchen. 3D Printing in Concrete. Additive Manufacturing at TUM, https://www.youtube.com/watch?v=H3aD0VZ3ESU (accessed on 3 October 2024).

[52] O.Fischer,D.Volkmer,P.Lauff,M.Hambach,M. Rutzen, Zementgebundener Kohlenstofffaserverstärkter Hochleistungswerkstoff (Carbonkurzfaserbeton); Forschungsinitiative Zukunft Bau, Band F 3178; Fraunhofer IRB Verlag: Stuttgart, Germany, 2019.

[53] P.Lauff,O. Fischer, Effizienter Ultrahochleistungsbeton mit innovativer trajektorienorientierter „Bewehrung “,*Ce Pap.*3 (2019) 82–88. doi.org/10.1002/cepa.976